Available online at www.sciencedirect.com
ScienceDirect
Journal of Volcanology and Geothermal Research 159 (2007) 246–266
Journal of volcanology and geothermal research
www.elsevier.com/locate/jvolgeores

Growth of an emergent tuff cone: Fragmentation and depositional processes recorded in the Capelas tuff cone, São Miguel, Azores

Henrik Solgevik [a,*], Hannes B. Mattsson [a,b,*], Otto Hermelin [a]

[a] *Department of Geology and Geochemistry, Stockholm University, S-106 91 Stockholm, Sweden*
[b] *Nordic Volcanological Center, Institute of Earth Sciences, University of Iceland, Askja, Sturlugata 7, IS-101 Reykjavik, Iceland*

Received 10 December 2004; accepted 11 June 2006
Available online 20 September 2006

Abstract

The Capelas tuff cone is an emergent Surtseyan-type tuff cone that erupted in shallow seawater off the coast of São Miguel, Azores. In this paper, we present a detailed stratigraphic study which is used to infer depositional processes and modes of fragmentation for the Capelas tuff cone deposits. The growth of the tuff cone can be divided into three stages based on variations in depositional processes that are probably related to differences in water/magma (W/M) ratios. The first stage corresponds well to wet Surtseyan-type activity where wet fallout is the dominant depositional process, with only minor representation of pyroclastic surge deposits. The second stage of the eruption is suggested to be the result of alternating wet and slightly drier periods of Surtseyan activity, with an overall lower W/M-ratio compared to the first stage. The drier Surtseyan periods are characterized by the presence of minor grain-flow deposits and undulating pyroclastic surge deposits that occasionally display relatively dry structures such as strongly grain-segregated layers and brittle behavior when impacted by ballistic ejecta. The first deposits of the second stage show an intense activity of pyroclastic surges but fallout, commonly modified by surges, is still the dominant depositional process during the second stage. The third stage represents a final effusive period, with the build-up of a scoria cone and ponded lava flows inside the tuff cone crater.

Phreatomagmatic fragmentation, as seen by studies of the fine ash fraction (<64 μm), is dominant in the Capelas tuff cone. However, particles with shapes and vesicularities characteristic of magmatic fragmentation are abundant in proximal deposits and present in all investigated beds (in various amounts). Emergent Surtseyan-type tuff cones are characterized by a domination of fallout deposits, both wet and dry, where dry periods are characterized by the deposition of relatively dry falling tephra transforming into grain-flow deposits. However, this study of the Capelas tuff cone shows that drier Surtseyan periods may also be represented by an increased amount of thin surge deposits that occasionally display dry features.

Keywords: Azores; tuff cone; phreatomagmatic; Surtseyan; depositional processes; facies; Scanning Electron Microscopy

1. Introduction

Monogenetic volcano fields occur in a variety of geological settings (Walker, 2000; Németh et al., 2003) and consist of volcanic landforms and products produced during single eruptions over a relative short time span. Products of such fields include scoria cones, small lava flows, tuff rings, tuff cones and maars (White, 1991; Walker, 2000; Connor and Conway, 2000). One of the main factors controlling the morphology of the resultant landform is the amount of external water present at the time of eruption (Sheridan and Wohletz, 1983; Wohletz

* Corresponding authors.
E-mail addresses: henrik.solgevik@geo.su.se (H. Solgevik), hannesm@hi.is (H.B. Mattsson).

0377-0273/$ - see front matter © 2006 Elsevier B.V. All rights reserved.
doi:10.1016/j.jvolgeores.2006.06.020

and Sheridan, 1983; Wohletz and McQueen, 1984; Lorenz, 1986; Sohn, 1996; Vespermann and Schmincke, 2000). Eruptions occurring in well-drained areas generally produce scoria cones, whereas maars and tuff rings/cones are produced by explosive phreatomagmatic eruptions as the result from magma interaction with ground- and/or surface-water (Wood, 1980; Wohletz and Sheridan, 1983; White, 1991). Eruptions that emerge through standing water generally produces tuff cones and are commonly termed Surtseyan eruptions, after the eruption of Surtsey 1963–1967 (Thorarinsson et al., 1964; Kokelaar, 1983; Moore, 1985; Sohn and Chough, 1992, 1993; Cole et al., 2001). Tuff cone-forming eruptions are characterized by a domination of fallout deposits, resulting in steep cone morphology and a high aspect ratio (i.e. height/crater diameter; Wohletz and Sheridan, 1983) (Thorarinsson et al., 1964; Sohn and Chough, 1992, 1993; Sohn, 1996; Vespermann and Schmincke, 2000). Tuff rings are suggested to consist mainly of base-surge deposits resulting in low angle ring morphology and a low aspect ratio (Wohletz and Sheridan, 1983; Sohn, 1996; Vespermann and Schmincke, 2000). The resultant morphology of the pyroclastic construct is directly controlled by depositional processes (Sohn, 1996), which are in turn controlled by a number of combined factors such as the properties, behavior, premixing, and mass-ratios of water and magma, vent geometry and physical properties of the surrounding bedrock (Kokelaar, 1986; Sohn, 1996; Vespermann and Schmincke, 2000; White and Houghton, 2000). Several studies have shown that a phreatomagmatic landform may consist of both tuff ring and tuff cone deposits due to changes in eruption style and depositional processes (Aranda-Gómez and Luhr, 1996; Sohn and Park, 2005). Thus, several factors need to be considered when classifying a phreatomagmatic landform. It is therefore essential to make more detailed stratigraphic studies of tuff cones/rings in order to consider what causes the observed variation in the deposits during growth, and finally to achieve a common classification scheme for phreatomagmatic landforms.

This study aims to identify various characteristic sedimentary deposits occurring in a well-exposed and nearly complete diagonal sequence of the Capelas tuff cone in order to deduce the processes responsible for the growth of the tuff cone. The tuff cone does not have any other rings/cones or maar-structures in the immediate vicinity and we thus infer a single vent to be responsible for the investigated deposit. We use morphology and textures of ash-particles, determined using images

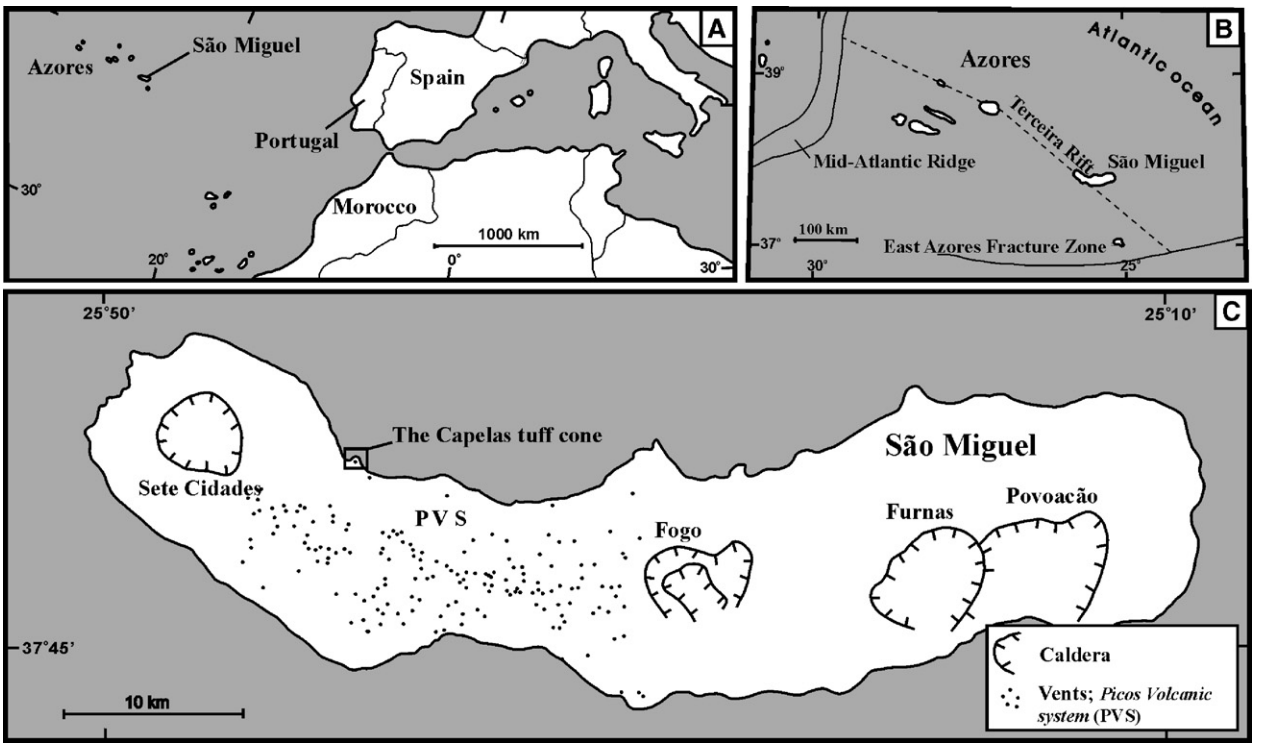

Fig. 1. Map showing (A) the location of the Azores (B) the Azores archipelago in relations to the Mid-Atlantic Ridge (MAR) and the Terceira Rift (C) the island of Sao Miguel with position of the Capelas tuff cone and Picos Volcanic System (PVS) (maps modified after Moore, 1990).

produced by Scanning Electron Microscopy (SEM), to study the fragmentation mode and grain modification from the eruptive processes during the growth of the cone (Sheridan and Marshall, 1983; Wohletz, 1983; Heiken and Wohletz, 1985; Wohletz, 1987; Büttner et al., 1999; Dellino et al., 2001).

2. Geological setting and general description of the tuff cone

The Capelas tuff cone is located on the northern coast of São Miguel, which is the largest island in the Azores archipelago (Fig. 1A and B). The Azores comprises nine islands situated near the Mid-Atlantic Ridge (MAR), close to the triple junction of the North American, Eurasian and African plates (Searle, 1980; Madeira and Ribeiro, 1990; Vogt and Jung, 2004). São Miguel is 63 km long and 8–15 km wide (Fig. 1C), and consists of several volcanically active areas (Moore, 1990; Cole et al., 1995; Jónsson et al., 1999), with five eruptions during the past 500 years (Moore, 1990) and ongoing fumarolic activity (Guest et al., 1999). The Capelas tuff cone belongs to the Picos Volcanic System (PVS; Fig. 1C). The PVS is a monogenetic volcano field connecting two larger trachytic central volcanoes, Sete Cidades in the west and Fogo (also known as Agua de Pau) in the east (Fig. 1C). The area has previously been referred to as Zone 2 by Moore (1990) and the "waist" region by Storey et al. (1989) and Guest et al. (1999). PVS is the youngest region on the island, dominated by Holocene basaltic eruptions related to the active NW–SE trending Terceira Rift (Fig. 1B) that crosscuts the western flank of São Miguel (Moore, 1990; Vogt and Jung, 2004). The age of the Capelas tuff cone is poorly constrained with age estimates ranging from 3.5 ky to 30 ky (Moore, 1990; Scarth and Tanguy, 2001).

The Capelas tuff cone (Fig. 2) is covered by alternating trachytic pumice and soil layers on its southwestern flank, whereas the southern and eastern flanks are overlain by a ~ 1.3 ka old basanitic lava flow (Moore, 1990). Units underlying the tuff cone (lava lobes and a ~ 2 m thick layer of trachytic pumice of fall origin) are exposed near sea-level on the western flank. The vent is located about 400 m off the old coastline, with the present-day crater floor situated 55 m above sea-level. The crater rim diameter is 650–700 m and the height of the rim is 107 m (a.s.l.). The aspect ratio (i.e. height/rim diameter) of the Capelas cone is 0.15, which is similar to many other tuff cones worldwide (Wohletz and Sheridan, 1983). Lapilli and ash are the dominant grain sizes present in the cone, although minor amounts of blocks and bombs exist (<5% of the total volume). Ballistic ejecta, commonly with impact-sag structures, are generally confined to specific

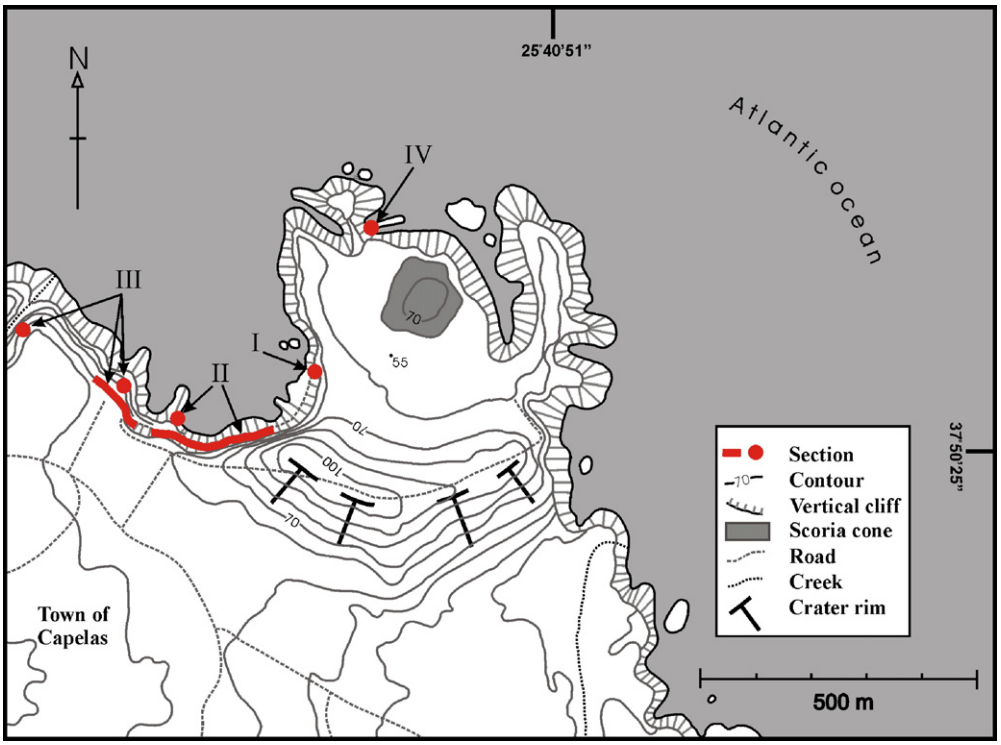

Fig. 2. The Capelas tuff cone. Roman numbers, I–IV, show locations of measurement for sections of the tuff cone.

layers within the cone. Beds are generally plane-parallel and dip radially up to 31° away from the crater, shifting to 1–6° down-section on the western flank. Pre-existing topography causes the distal parts of the tuff cone to dip toward the crater (Fig. 3). Synvolcanic ring-faulting and slumping is visible on the rim and inside the crater rim in the northwest and northeast area, causing late deposits to dip steeply into the crater (>30°) with marked unconformities between early and late deposits. A Strombolian scoria cone and associated lava pond inside the crater represent the effusive ending of the eruption. Marine erosion, probably both syn- and post eruptive, has reduced the original tuff cone volume by about 50%.

3. Methods

In the field, a total of nineteen stratigraphic logs were measured, with increasing distance from the vent, on the western side of the Capelas tuff cone (Fig. 2). This was made possible by a small road connecting the town of Capelas with the small fishing port located at sea-level near the center of the cone (Fig. 3). The road-cut stretches from distal late-stage deposits down to the early proximal deposits allowing for a near complete eruptive sequence to be studied in detail. The stratigraphic logs were collected from four sections (I) proximal deposits, (II) medial deposits, (III) distal flank deposits, and (IV) inside the crater (Figs. 2 and 3). When possible, the upper bed of a log was traced horizontally and represents the lowest bed of the next log. Inaccessible parts of the stratigraphic logs were examined by photographs and in the field using binoculars. Deposits were divided into sedimentary facies based on grain size, sedimentary structures and bed geometry. Estimates of grain sizes were conducted in field using a comparative grain size chart. Sieving was not possible due to the moderate consolidation/palagonitization of the deposits. The grain size classification is modified after Chough and Sohn (1990) due to field conditions and comprises ash (<2 mm), fine lapilli (2–16 mm), coarse lapilli (16–64 mm) and blocks/bombs (>64 mm).

Scanning Electron Microscopy (SEM) and Energy Dispersive System (EDS) analyses were conducted at Stockholm University using a Philips XL30 ESEM-FEG instrument. SEM-images were produced in low-pressure vacuum, with a backscatter detector at 20 kV. The EDS-analysis was performed at 25 kV, using spot mode. Samples for SEM-imaging and EDS-analyses were prepared according to Sheridan and Marshall (1983). However, the samples were not crushed or sieved prior to SEM-analysis due to moderate consolidation/palagonitization. Instead, a square centimeter surface of each sample was studied and images

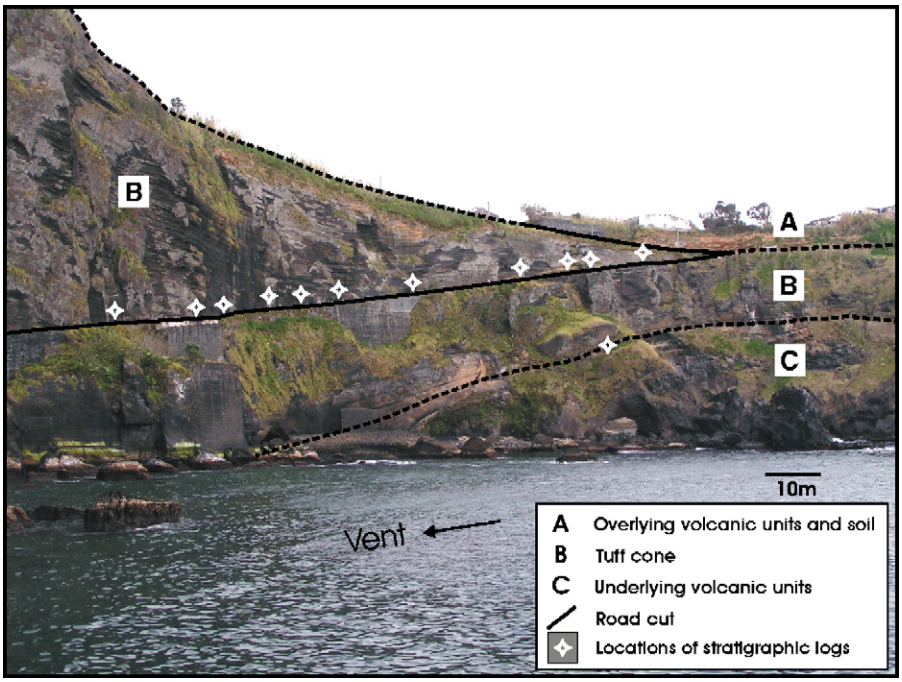

Fig. 3. Southwest exposure of the Capelas tuff cone with the road-cut from distal flank deposits down to proximal deposits showing locations for log-measurements in section II and partly section III. Picture taken looking towards SSW.

produced of representative particles within that area. Two sizes of juvenile glass particles were studied in detail. First, grain sizes ≤ 64 μm (fine ash) were used to study the mode of fragmentation (Dellino and La Volpe, 1995; Zimanowski et al., 2003). Second, particles larger than 64 μm (coarse ash) were complemented to the study of fragmentation mode as well as for surface and morphological changes due to transport and deposition (Sheridan and Marshall, 1983; Wohletz, 1987). Morphological parameters were classified following Dellino et al. (2001). Semi-quantitative chemical analyses (using EDS) were conducted on selected particles in SEM images to verify that descriptions and interpretations were carried out on juvenile glass particles and not on crystals or accidental lithic fragments.

4. Facies descriptions and interpretation

Eight sedimentary facies were identified in the Capelas tuff cone (Table 1). The classification into different

Table 1
Summary and brief descriptions of sedimentary facies

Facies	Brief description/ characteristics	Main location in tuff cone	Interpretation
A. Planar grain supported lapilli	Planar continuous bedding with a pinch-and-swell of 9–12 cm, grain supported lapilli with common open framework, structureless, erosive basal contact, rare blocks and bombs <7 cm.	Base of tuff cone	Explosion breccia deposited by a pyroclastic flow
B. Lapilli lenses	Lenticular beds, grain supported lapilli-ash, structureless or reverse-graded both vertically and down slope, length varies between dm and m, thickness rarely exceeds 15 cm.	Steep slopes and slope break	Grain flow from falling pyroclasts. Fallout from continuous uprush or jets of relatively dry tephra
C. Planar stratified deposits	Laterally consistent planar bedding, dominantly ash-lapilli, alternating coarse/fine grained continuous internal layers (normally thinning upwards, structureless or graded layering, bed thickness 4.5–83 cm, internal layers mm–cm thick, generally moderately sorted and matrix supported.	Medial to distal flank deposits	Traction and suspension from low concentration pyroclastic surge and fallout when showing normal grading and mantling
D. Diffuse stratified deposits	Laterally consistent planar bedding (rare pinch-and-swell), ash-lapilli to lapilli-ash, continuous and discontinuous (lapilli-trains or ash-rich) internal layers, structureless or graded, occasional blocks/bombs with few impact-sags. bed thickness 4.5–53 cm (average 20 cm), moderately sorted.	Medial deposits	Carpet traction from pyroclastic surge and/or fallout from tephra jets or continuous uprush with subsequent tractional transport
E. Crudely stratified deposits	Laterally consistent planar bedding, lapilli-ash (>10% visible coarse lapilli), massive to weakly stratified (discontinuous internal layers), commonly blocks/bombs and impact-sags, bed thickness up to 180 cm (average 30 cm), commonly poorly sorted.	Proximal to medial deposits	Fallout from dense tephra jets and continuous uprush or carpet traction from a highly concentrated pyroclastic surge
F. Massive to stratified ash	Thin beds to laminae (normally 1–5 cm), planar and continuous, massive to stratified (F.b. generally stratified), predominantly ash (generally well sorted), rare fine lapilli horizons. F.a.: mantling topography F.b.: thickens in depressions and thins over highs	F.a. medial to distal flank. F.b. ubiquitous	F.a. fallout, co-surge fall F.b. dilute pyroclastic surges
G. Undulating ash beds	Laterally continuous beds with pinch-and-swell structures and undulating lamination, predominantly ash. Internal lenses, rare ripples and cross-lamination in medial to distal flank deposits, bed thickness 2.5–40 cm (average 5–10 cm).	Medial deposits	Low concentration pyroclastic surge
H. Massive muddy ash and lapilli	Compact muddy deposits, planar to irregular boundaries, moderate to poorly sorted, matrix supported, structureless to reverse-graded. H.a.: lenses, ash-lapilli, thickness 5–25 cm, dm–m's long, H.b.: filling in depressions, lapilli-ash	Slope break and depression filling	Debris/mud flow

facies is based on variations in grain size, sedimentary structures and bed geometry. In the following subsections we present the characteristics, main location and interpretation of each facies. Individual facies represent a fixed point in a spectra of process continuum. That is, any single process might change in space and time as a result of variations in physical parameters and therefore can produce different sedimentary facies at various stages of evolution (Wohletz and Sheridan, 1979; Fisher and Schmincke, 1984; Sohn and Chough, 1989; Chough and Sohn, 1990). This can result in difficulties in classifying a deposit into a specific facies if it represents an intermediate stage between two end-members/facies. For example, there is a continuum between Facies D and E with respect to grain size and the presence or absence of continuous internal layers, between C and D with respect to the amount of grain segregation and distinct continuous internal layering and between Facies F and G with respect to the presence of undulating beds and laminae.

4.1. Facies A — planar grain supported lapilli

The planar grain supported lapilli facies is characterized by continuous planar bedding of coarse lapilli displaying slight pinch-and-swell structures, with embedded angular blocks and bombs (Fig. 4A and Table 1). There is a small, but clear, density variation of clast types with distance from the vent. Facies A in the medial section of the cone contains juvenile material (46%), pumiceous lithic clasts (32%) and dense accidental lithic fragments (22%). The distal section contains less juvenile material (−3%), and dense accidental lithic fragments (−13%), whereas the relative abundance of pumiceous clasts increases (+16%). Pumice fragments have abraded edges, whereas dense accidental lithics clasts are sharp and angular. The lowermost part of the layer consists of a ~ 3 cm thick ash layer into which the coarse clasts are intimately imbedded. This facies is only found at the base of the cone at distances between 300 m and 700 m from the vent. The same facies probably

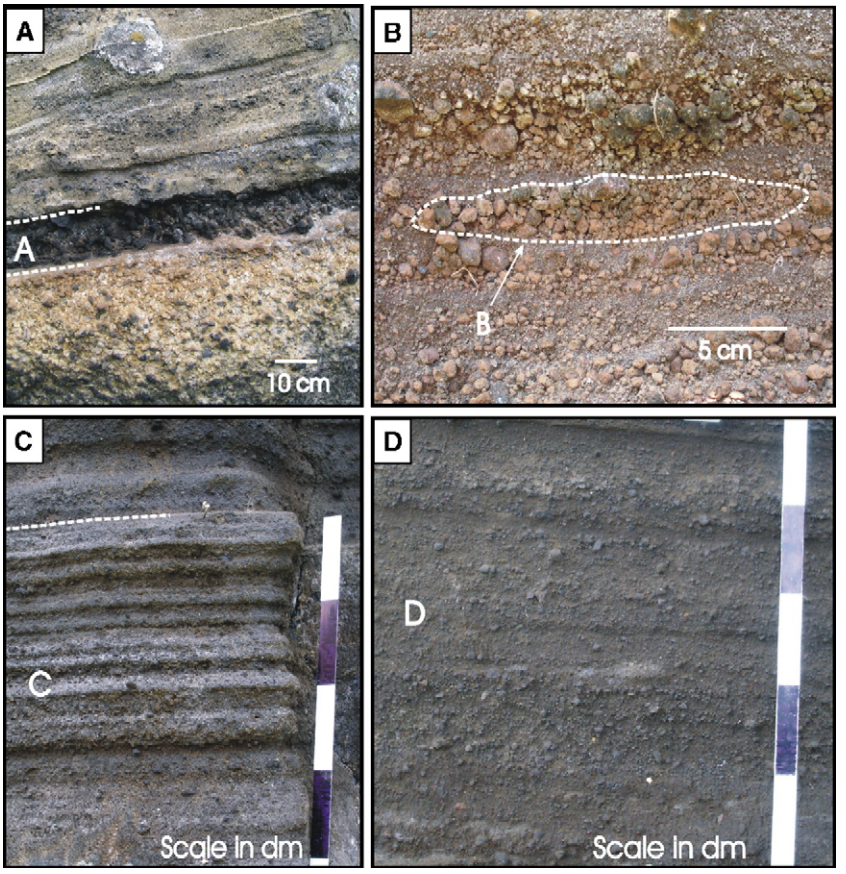

Fig. 4. (A) Facies A, planar grain supported lapilli (B) Facies B, lapilli lenses occurring in steep dipping strata (~ 38°) inside the crater rim (C) Facies C, planar stratified deposits with structureless internal layering showing a thinning upward sequence. (D) Facies D, diffuse stratified deposits, medial section. Vent is to the left in all pictures.

continues closer to the vent but the basal part of the tuff cone is currently below sea-level.

Interpretation: Coarse lapilli and blocks and bombs of angular to subangular shape with similar size and of widely different characteristics suggest that this facies is a breccia generated by explosive activity associated with deepening and widening of the vent. Several lines of evidence suggest that the explosion breccia was emplaced by a high-density pyroclastic flow or a particle-laden surge. This interpretation is based on: (1) the erosive basal contact, (2) the slight, but consistent, pinch-and-swell structure, (3) the ash embedded in the layer, which is believed to be the result of a ground-surge deposited in front of the main flow body (Druitt, 1998) or associated fallout ash percolating through the open framework of the explosion breccia clasts, (4) the variation in clast types with distance from the vent, with denser ejecta closer to the vent and an increase in the amount of semi-rounded pumiceous and juvenile clasts with distance. If this was the result of an explosion expelling dense lithic clasts and pumiceous material of similar size and deposit them through tephra fall, the denser clasts would gain more momentum and be less susceptible to drag-forces during flight than the light pumiceous material. Similar explosion breccias, containing a mixture of angular fragments from underlying strata, occurring near the base of tuff cones and tuff rings have previously been briefly discussed by Wohletz and Sheridan (1983).

4.2. Facies B — lapilli lenses

This facies consists of lenticular layers of grain-supported fine to coarse lapilli, which commonly display an open framework (Fig. 4B and Table 1). The lapilli lenses are either structureless or reversely graded, with slight coarsening down slope. Lenses generally pinch out, but occasionally display blunt terminations down slope. Lapilli lenses occur as single lenses on gentle slopes and as clusters in crudely stratified deposits on steep slopes. On gentle slopes, lapilli lenses are generally long (up to 150 cm) and thick (up to 15 cm) and commonly display a positive relief on the upper surface and a non-erosional lower contact. On steep slopes, on the other hand, lapilli lenses are shorter and thinner than their gentle slope equivalents. The steep slope lenses also commonly display a biconvex appearance (due to an oblique view of the flow direction) and more diffuse contacts with other facies.

Interpretation: Lapilli lenses occurring in steep rim beds showing reverse grading (and coarsening down slope) are indicative of "freezing" deposits of grain flow transportation that have evolved from falling pyroclasts (Sohn and Chough, 1992, 1993). The open framework, depleted of the fine fraction, further indicates a relatively dry environment that probably enhanced grain segregation and development of reverse graded structures. Lenses inside the crater are embedded in crudely stratified deposits (Facies E) suggesting that in drier conditions, the crudely stratified deposits could separate out/evolve into clusters of lapilli lenses. Lapilli lenses at gentle slopes are interpreted as being deposits of grain flows, but with "freezing" due to rapid energy loss at slope breaks or by entering a water-soaked depression rather than "freezing" (as on steep slopes) due to continuous supply of relative dry falling tephra. Based on these assumptions we suggest that single lenses on gentle slopes are deposits of relatively dry tephra jets that may evolve into a debris-flow if the flow enters wet ground conditions or if the flow has higher water content, as indicated by Sumita et al. (2004).

4.3. Facies C — planar stratified deposits

Planar stratified deposits are defined by laterally consistent planar bedding with continuous internal stratification (Table 1). The planar stratified deposits are generally moderately sorted and matrix supported lapilli-ash that fines away from the vent. Internal stratification is characterized by alternating structureless fine lapilli-rich and ash-rich layers (Fig. 4C), or by alternating graded layers. Internal layers are predominantly reversely graded in the medial section, whereas normally graded layers increase in the distal flank deposits. Upper surfaces show plastic deformation when impacted by ballistic ejecta. Internal boundaries range from sharp to gradational or diffuse. This facies occurs in medial deposits (<10° dip) and in distal flank deposits (<12° dip).

Interpretation: Laterally planar stratified deposits with internal layering of alternating fine lapilli-rich and ash-rich layers of graded or structureless layers have been interpreted by some workers as fallout deposits (e.g. Cole et al., 2001) and by some workers as pyroclastic surge and co-surge fallout deposits (e.g. Wohletz and Sheridan, 1979; Fisher and Schmincke, 1984; Sohn, 1997; Dellino et al., 2004b). However, as emphasized by several workers (Verwoerd and Chevallier, 1987; Wilson and Hildreth, 1998; Valentine and Fisher, 2000; Cole et al., 2001), it can be difficult to separate surge deposits from wind-drifted fallout deposits in distal regions. We interpret planar stratified deposits as emplaced by pyroclastic surges when there is thickening in depressions and a thinning upward

internal sequence (Sohn and Chough, 1989; Sohn, 1997) and as fallout deposits when displaying normal grading that mantle topography (Crowe and Fisher, 1973; Fisher and Schmincke, 1984). Multiple massive layers showing alternation of strongly grain-segregated layers defined by a coarser grained (coarse ash to fine lapilli) lower layer (rarely reverse graded) topped by a finer grained (ash) layer are interpreted as a result of multiple closely spaced surges. One co-set of coarse and fine grained layers is suggested to represent a single surge (Sohn and Chough, 1989; Dellino et al., 2004a,b).

4.4. Facies D — diffuse stratified deposits

This facies is characterized by laterally consistent planar bedding with continuous to discontinuous internal stratification (Fig. 4D and Table 1). Discontinuous internal layers are either ash-rich or consist of fine lapilli trains, commonly not more than one grain thick. Armoured lapilli occur in very sparse quantities at one location in medial deposits. The uppermost part of this facies is commonly structureless but weak reverse grading is not uncommon when overlain by undulating ash beds (Facies G) or massive to stratified ash (Facies F). Basal contacts are commonly gradational toward crudely stratified deposits. Diffuse stratified deposits are present in all sections of the cone, but are most voluminous in the medial deposits.

Interpretation: This facies shows tractional structures defined by continuous and discontinuous internal layers visually separated by differences in grain size. Variable contacts between internal layers and rare reverse grading indicate internally changing depositional conditions such as high shear stress (Sohn and Chough, 1993), change in velocity, flow steadiness and particle concentration (Dellino et al., 2004a), all possibly related to a pulsing turbulence (Carey, 1991). These parameters imply emplacement by a pyroclastic density current with traction and suspension sedimentation. However, the continuous planar bedding indicates emplacement by fallout (Cole et al., 2001). Diffuse stratified deposits found in proximal and medial deposits are interpreted as emplaced more or less simultaneously by pyroclastic surges and a relatively high concentration tephra fall with subsequent tractional transportation. Cole et al. (2001) interpreted similar deposits at the Capelinhos tuff cone as surge-modified fall deposits. Diffuse stratified deposits found in medial deposits where the strata dip gently (<10°) toward the crater and in distal flank deposits are interpreted as the result of a traction carpet sedimentation driven by a pyroclastic surge. Tephra fall deposits with subsequent tractional transportation would probably have lost their gravity momentum at the slope break and would not be able to segregate internal layers farther away.

4.5. Facies E — crudely stratified deposits

Crudely stratified deposits are characterized by laterally consistent planar bedding of weakly stratified to massive deposits (Fig. 5A and Table 1). Discontinuous and rare continuous ungraded or weakly reverse graded internal layers define the stratification. Facies E consists of subrounded to subangular lapilli-ash with >10% visible coarse lapilli. Ballistic ejecta (<28 cm) and impact sags (<1 m deep) are common in medial and distal flank deposits and occur both at the base and inside the deposits. Occasional bombs with a cow-pat morphology occur in proximal deposits. Early proximal deposits contain well-rounded pebbles, shell fragments from marine molluscs and up to 30% pumice lapilli fragments. Basal contacts are generally erosional. Beds with few blocks and/or bombs and several discontinuous internal layers might appear similar to diffuse stratified deposits, but crudely stratified deposits are distinguished from Facies D by larger grain size (i.e. >10% visible coarse lapilli). In steeply dipping strata (e.g. inside the crater rim and in proximal deposits), crudely stratified deposits also contain clusters of lapilli lenses (Facies B).

Interpretation: Crudely stratified deposits are interpreted as being deposits of two different emplacement mechanisms, (1) rapid emplacement from high concentration pyroclastic tephra fall either lacking or showing weak tractional transport or (2) a traction carpet under a highly concentrated pyroclastic surge. The erosion of underlying undulating beds (Facies G) in proximal deposits indicate a rapid pile-up and mass-loading at a slightly oblique angle of pyroclastic fall deposits, probably the result of dense wet tephra jets (Kokelaar, 1986; Sohn and Chough, 1992) or continuous uprush activity. The latter is described to be responsible for the most rapid accumulation of tephra at the eruption of Surtsey 1963–1967 (Thorarinsson et al., 1964; Thorarinsson, 1967; Kokelaar, 1983; Moore, 1985; Kokelaar, 1986). Both processes include plucking of pre-existing unconsolidated marine sediment. Crudely stratified deposits containing more pronounced tractional transport are interpreted as deposits from a traction carpet in a highly concentrated pyroclastic surge (Sohn and Chough, 1989, 1992; Sohn, 1997; Németh et al., 2001), occasionally occurring in a vertical relation with planar stratified deposits (Facies C) and undulating deposits (Facies G). Blocks/bombs and impact sags in

basal parts of a bed are indicative of ballistically emplaced ejecta from initial explosions prior to tephra jetting and/or base surge development (Waters and Fisher, 1971; Kokelaar, 1983; Moore, 1985; Cole et al., 2001), whereas internally occurring bomb/impact sags might be the result from single or closely spaced tephra jet explosions occurring contemporaneously with the progressing surge (White and Houghton, 2000) or, according to Sohn and Chough (1989), as the result from multiple amalgamated beds deposited by several separate events.

4.6. Facies F — massive to stratified ash

This facies is characterized by thinly bedded to laminated deposits of massive or planar stratified ash (Table 1). It occurs as single units or in a set of beds or laminae. Beds and laminae are commonly planar and continuous and either follow topography (subfacies F.a.; Fig. 5B) or thicken slightly in depressions and thin over highs and edges (subfacies F.b.). Internal stratification is caused by variations in grain size or color and are either diffuse or show planar continuous layers rarely exhibiting grading. Massive deposits less than 1.5 cm thick are commonly intercalated with stratified deposits (Facies C, D and E) or between beds. Massive ash deposits commonly display sharp contacts. Both F.a. and F.b. are often associated with undulating ash beds (Facies G) showing gradational contacts and, in some cases, constituting the core of an undulating ash bed. F.a. is most common in medial to distal flank whereas F.b. commonly occurs from proximal to distal deposits of the tuff cone.

Interpretation: Continuous bedding and mantling of irregularities (subfacies F.a) are characteristics of fallout deposits (e.g. Houghton et al., 2000; Cole et al., 2001; Schmincke, 2004). Fallout deposits of this facies are probably the result of both plumes and co-surge

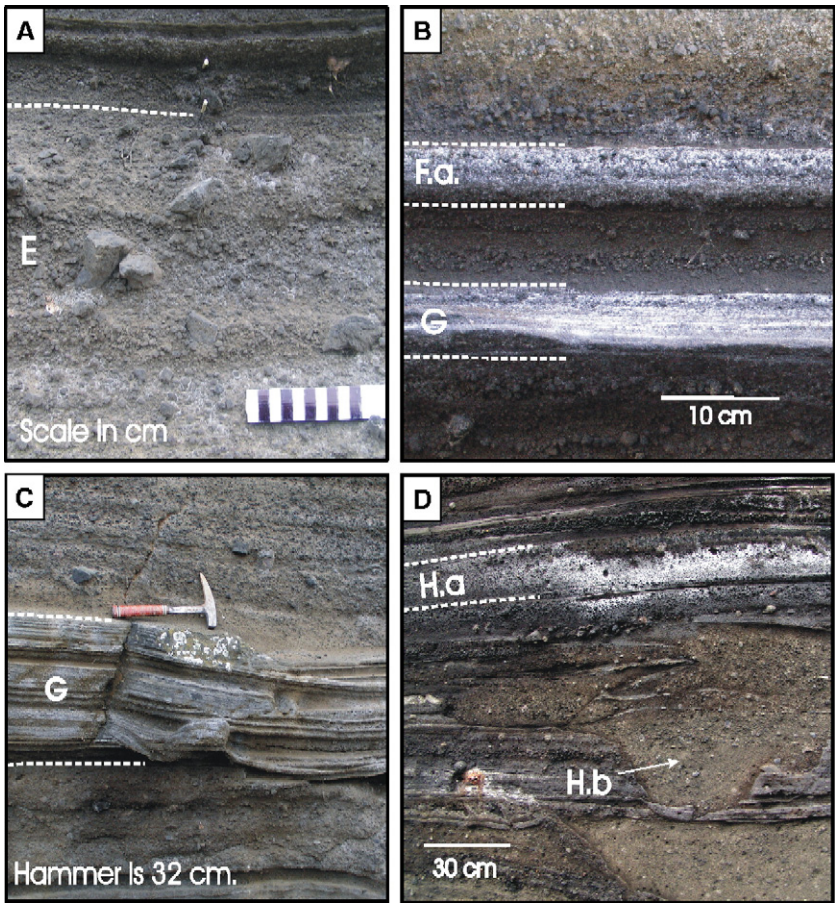

Fig. 5. (A) Facies E, crudely stratified deposits, medial section (B) Facies F, showing mantling massive ash (F.a.) (C) Facies G, undulating ash beds (D) Facies H, massive muddy ash and lapilli, showing lenses (H.a) and infilling deposits (H.b) with a weak basal stratification in infilling deposits. Vent is to the left in all pictures.

fallout. Co-surge fallout deposits are indicated when massive or stratified ashes overlie undulating ash beds (Walker, 1984; Sohn, 1997; Valentine and Fisher, 2000; Dellino et al., 2004a,b). The existence of thickening in depressions and thinning over highs and edges (subfacies F.b.) suggests lateral movement where the differences in flow power and shear stress could be traced with a variety of asymmetric or symmetric infilling structures in depressions (Chough and Sohn, 1990). Small grain size, common stratification and variation in thickness over highs and depressions suggest that subfacies F.b is a deposit of a low concentration pyroclastic surge (Crowe and Fisher, 1973; Sohn and Chough, 1989; Chough and Sohn, 1990; Sohn and Chough, 1992; Németh et al., 2001), probably in a dilute waning stage.

4.7. Facies G — undulating ash beds

Laterally continuous beds with pinch-and-swell structures and undulating laminations are characteristic for this facies (Fig. 5B and C, Table 1). Internal lamination is either continuous or discontinuous and may display weak normal grading. Internal undulations are commonly more pronounced than the external pinch-and-swell structure. Internal lenses are commonly present in medial to distal flank deposits, >350 m from the vent. Lenses are up to 120 cm long and up to 5 cm thick and commonly consist of ash and scarce fine lapilli and coated/rimmed with finer grained ash. Low angle cross-lamination and on-lapping structures are apparent in internal scoured troughs, or when several internal lenses are closely spaced. Rare ripples, about 20 cm long and 2–3 cm high, are found on the upper contact. Stoss-side angle is up to 9° and lee-side angle varies between 30° and 90°. Accumulation of coarser ash and/or lapilli is found on the lee side of ripples. Only a few sand-wave structures (with wavelengths of approximately 1.3 m and wave height around 10 cm) are exposed in the tuff cone and are present at the basal part of the thickest undulating bed with gently dipping stoss sides and slightly steeper lee sides. Some beds display brittle rupture when impacted by ballistic ejecta. Undulating stratified beds increase toward the vent, whereas distinct lamination, internal lenses, cross-lamination and sand-wave structures first appear in the medial deposits, i.e. >350 m from the vent.

Interpretation: Undulating ash beds are interpreted as deposits from base surges based on the presence of ripples, dunes, internal lenses and low angle cross-stratification. This interpretation coincides with several previous studies on similar deposits, e.g. Waters and Fisher (1971), Crowe and Fisher (1973), Cole (1991), Cole et al. (2001), Sohn and Chough (1989), Chough and Sohn (1990), De Rosa et al. (1992) and Dellino et al. (2004b). However, there is an increase of undulating ash beds, not showing any bedform structures except weak stratification, toward the vent. Different kind of bedform structures in base-surge deposits have been suggested to be the result of variations in flow regime (Valentine and Fisher, 2000) and particle concentration in base surges (Sohn and Chough, 1989; Sohn, 1996) where ripples are the result of low flow regime and dunes to an increase in flow regime (Fisher and Schmincke, 1984; Valentine and Fisher, 2000). Pyroclastic surges may occur as wet or dry events depending on the temperature. Temperatures below 100 °C generally produce “wet” three-phase surges and above 100 °C “dry” two-phase surges (Carey, 1991; Druitt, 1998; Valentine and Fisher, 2000). Lorenz (1974a,b), Walker (1984) and Sohn and Chough (1992) interpreted the presence of accretionary and armoured lapilli as well as the plastering of ash onto objects, as indicative of wet surges. Valentine and Fisher (2000) further reviewed that wet surge deposits tend to be more poorly sorted than those of dry surges, consist of steep-sided bed forms due to the cohesion (compared to low angle stratification common in dry surges) and act plastically when impacted by ballistic ejecta. The undulating tuff beds at the Capelas tuff cone display steep lee sides (30°–90°) on ripples and generally display plastically deformed beds by impacts, yet display low angle stratification and an absence of accretionary and armoured lapilli. This would suggest that the undulating ash beds, Facies G, consist of both wet and dry base-surge deposits with a domination of the former. These surge deposits are suggested to have formed during varying temperatures in relatively low energy surges.

4.8. Facies H — massive muddy ash and lapilli

The massive muddy deposits consist predominantly of structureless or reverse graded ash and lapilli (Table 1). This facies have a compact appearance with sharp boundaries and occurs as lenses at slope breaks (subfacies H.a.), or as filling (subfacies H.b.) in depressions (Fig. 5D). Lenses (H.a.) mostly pinch out but in rare cases display blunt terminations with a thicker lobe down slope and a pinching out tail up slope. Smooth basal contacts are mostly concave (i.e. showing a positive relief; Fig. 5D), whereas irregular contacts have a convex nature. A small meandering flow structure, ~ 1 m long, 7–13 cm wide and 1–2 cm deep with steep edges, is exposed on the surface of the tuff cone dipping 21° outward. Subfacies H.

b. infill topographic depressions such as impact sags and V- or U-shaped channels. Infilling deposits and lenses with irregular erosive lower boundaries rarely contain randomly distributed well-rounded larger clasts (<4 cm), up to 5 vol.%. The lower parts of the infill deposits and irregular lenses rarely show a weak stratification, consisting of few stringers (<30 cm long) of slightly coarser particles than the matrix (Fig. 5D).

Interpretation: Massive muddy ash and lapilli lenses, H.a., are interpreted as debris-/mudflows based on the observed sharp boundaries and massive muddy appearance (Shultz, 1984) and including blunt terminations down slope with a pinching-out tail up slope and positive relief (Sohn and Chough, 1992, 1993). The presence of these lobe-like lenses entering depressions from both directions (e.g. both away and toward the crater) further supports the interpretation of debris/mudflows, and suggests an origin of remobilized wet tephra (Leat and Thompson, 1988; Sohn and Chough, 1992). The meandering structure on the surface of the outward steeply dipping strata corresponds well in geometry to the mudflow channels described from Surtsey by Lorenz (1974a,b). Deposits entering from the direction of the vent might also be emplaced by explosive expulsion from a wet vent-clearing slurry (Kokelaar, 1983) or the collapse of a condensed eruption column (Ross, 1986; Leat and Thompson, 1988). The variable grading is probably due to differences in water content and grain concentration reflecting variable flow strength and plasticity (Shultz, 1984). Some U-channels have steep sides and a geometry (Fig 5D), that better corresponds to the channel and tube structures developed by viscous density flows as described by Verwoerd and Chevallier (1987), rather than U-channels developed by base surges as described by Fisher (1977). Stream-rill-formed V-channels later smoothed out by base surges to form U-channel geometry and subsequently filled by multiple beds, occupy a horizon ~ 3 m above the base of the tuff cone, and is clearly exposed in distal flank deposits (Fig. 6).

5. Stratigraphy

5.1. Section I — proximal deposits

The first section (Fig. 7A and B) is located 200 to 350 m from the vent (Fig. 2). The most proximal deposits, situated at sea-level, dip ~ 12° away from the vent. Deposits at the border with section II, ~ 20 m above sea-level, decrease in dip to about ~ 6°. The proximal deposits generally exhibit thick to very thick bedding and an overall coarser grained character than medial and distal flank deposits (sections II and III, respectively). Proximal deposits are characterized by a domination of crudely stratified deposits (Facies E; Fig. 8, Table 2). Facies E is here represented with a relatively small amount of angular blocks and impact sags, showing only occasional cow-pat bombs. Well-rounded pebbles, shell fragments of marine molluscs and pumice fragments are

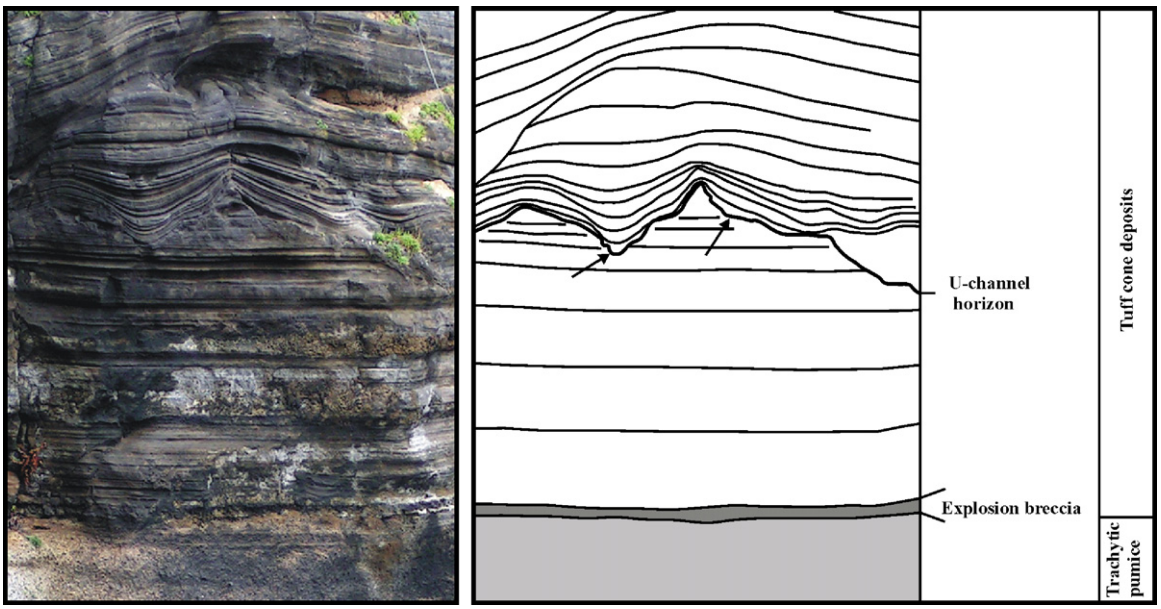

Fig. 6. Photograph and simplified sketch of the U-channel horizon located approximately 3 m above tuff cone base in the distal flank deposits. Arrows point at straight edges and areas not filled with pyroclastic deposits, suggesting initially stream-rill shaped channels. Looking SSW, away from the vent.

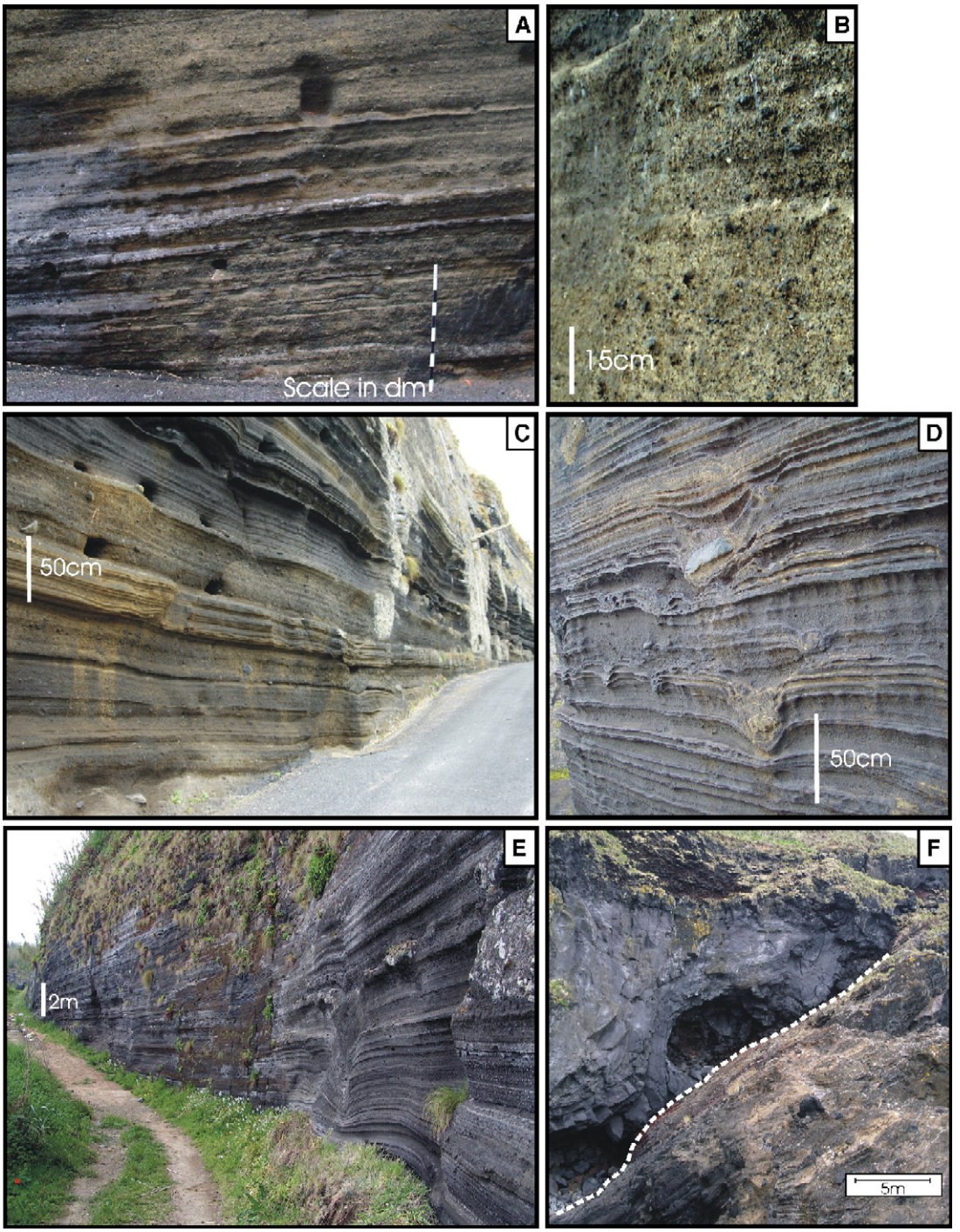

Fig. 7. Pictures showing (A) section I (B) close-up of Facies E, section I (C) section II, upper parts (D) section II, lower parts. Note the asymmetrical thickness of deposits filling the impact-sags indicating lateral transport. (E) section III (F) section IV overlain by lava pond. See also Figs. 2 and 8 for location of sections relative to the vent. The vent is to the right in picture A and B, obliquely forward to the left in picture C and to the left in picture F.

incorporated in crudely stratified deposits and represent products derived from underlying unconsolidated marine sediment. The proximal deposits at Capelas are interpreted to be the result of dense fallout deposits from tephra jets and continuous uprush with occasional surge development.

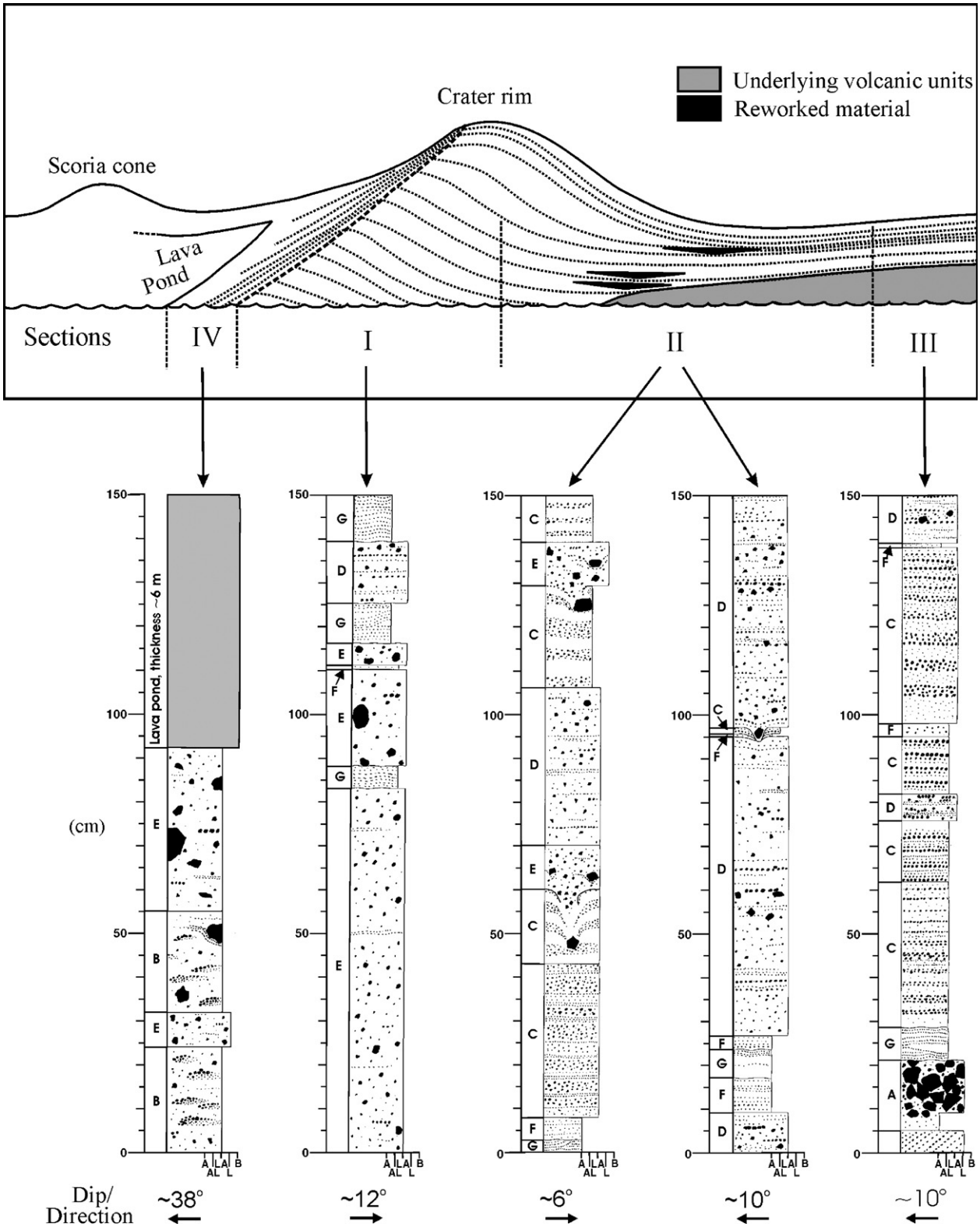

Fig. 8. Schematic illustration showing the western side of the Capelas tuff cone, and sections I–IV relative to the vent (scoria cone). The figure also shows representative stratigraphic logs from each section. Letters in the left column in the logs refer to facies. Section II is represented by two logs to distinguish between lower and higher deposits (see Fig. 7D and C, respectively). A = ash, AL = ash and lapilli, LA = lapilli and ash, L = lapilli, B = block/bomb.

Table 2
Facies distribution in volume percent (vol.%) for facies represented with 1% or more for each section and the total volume

Facies	Section				Total (vol.%)
	I	II	III	IV	
A	–	1	5	–	1
B	–	–	–	51	2
C	–	29	49	–	29
D	5	45	18	–	31
E	86	9	13	49	23
F	1	6	10	–	6
G	8	4	5	–	4
H	–	6	–	–	4

5.2. Section II — medial deposits

The second section comprises distances from 350 to 500 m from the vent (Figs. 2 and 8). Measurements were conducted diagonally through the cone from 20 m above sea-level (cone thickness ~ 100 m) and up to 45 m above sea-level (cone thickness ~ 20 m) (Figs. 3 and 8). In the first 100 m of the medial deposits beds dip ~ 6° away from the vent, which changes to a dip of between 6° and 10° (toward the vent) with increasing distance from the vent due to underlying topography. All eight facies are represented in this section (Figs. 7C, D and 8 and Table 2). Internal layers are commonly massive or reversely graded. The lower and proximal part of the section consists of several beds (planar stratified deposits, Facies C) with multiple layers of strongly grain-segregated deposits (Fig. 7D). The distal and upper part of the medial deposit change to an increase of diffuse stratified deposits (Facies D; Fig. 7C). In comparison with section I (proximal deposits), there is an increase in surge deposits. These surge deposits display several characteristics indicative of both dry and wet surges (see Section 4.7). Deposits of massive muddy ash and lapilli (Facies H) occur complexly interbedded with pyroclastic deposits in large lenses at slope breaks, up to 60 m long and 3 m thick, where the tuff cone deposits overlie pre-existing volcanic units causing the deposits to dip toward the vent (Fig. 8). The uppermost part of the cone, 70–110 m above sea-level, was not investigated in detail but deposits steeply dip (~ 30°) outward, display a mudflow channel on the surface (similar to Fig. 4 in Lorenz, 1974a,b) and rare beds with soft-sediment deformation structures. Medial

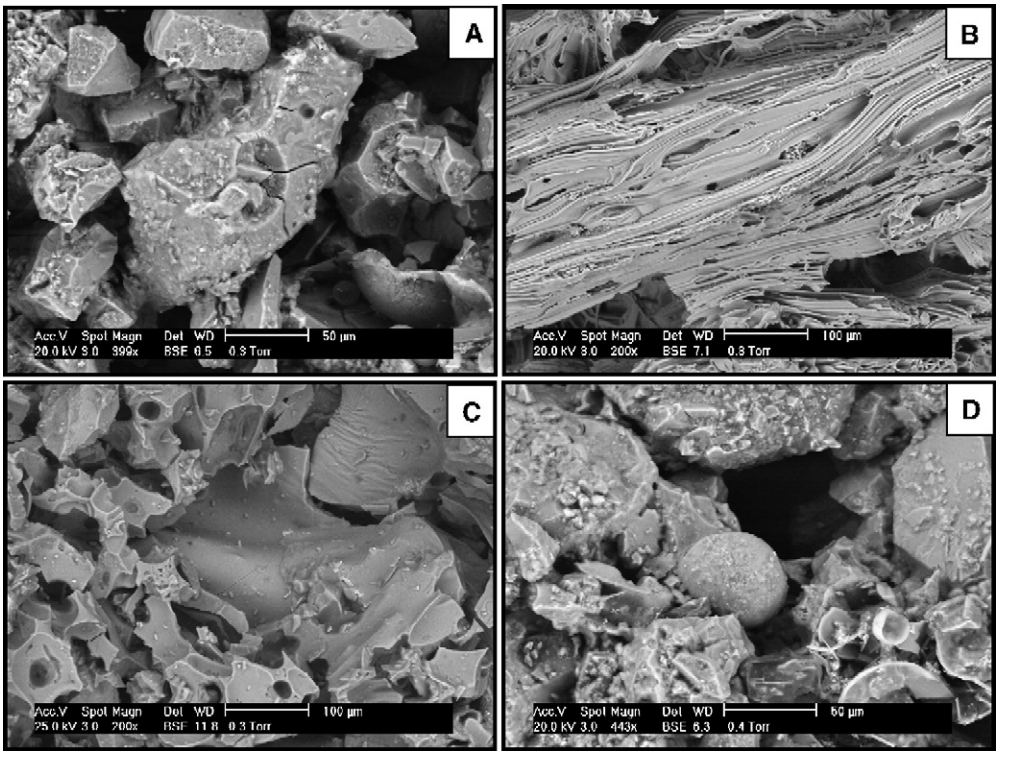

Fig. 9. SEM images displaying representative samples of (A) blocky and equant particles of fine ash and a larger angular particle with low vesicularity. Adhering particles occur on all grains. Facies F, medial section. (B) Underlying fallout deposits of trachytic pumice displaying a high vesicularity of tabular and contorted vesicles. Medial section. (C) Highly vesicular and irregular shaped juvenile clasts. Facies E, proximal deposits (D) Spherical particle indicating a ductile fragmentation, Facies F, medial deposit.

deposits are interpreted to be the result of generally surge-modified fallout deposits and debris/mud-flows (directly or indirectly) from tephra jets and continuous uprush, and from pyroclastic surges emanating from large-scale jetting and/or eruption column collapse.

5.3. Section III — distal flank deposits

The distal flank deposits (Fig. 7E) are found at distances exceeding 500 m from the vent (Figs. 2 and 8). Deposits dip ~ 4–16° toward the vent due to underlying topography and generally consist of planar- and diffuse stratified ash deposits (Facies C and D; Table 2). Internal layers are mostly massive or graded, and reversely and normally graded sequences occur at approximately equal abundance. U-channels are prominent along a distinct horizon about 3 m above the tuff cone base (Fig. 6). Distal flank deposits are interpreted to be deposits from fallout and pyroclastic surges with a variation from high concentrated bedload to a dilute waning stage with slow suspension sedimentation. Deposits from debris- and mudflows (Facies H) are not logged but constitute a minor quantity (<1%; Table 2) and are found in V- and U-channels. Undulating ash bed deposits rarely display brittle rupture when impacted by ballistic ejecta. The upper part of the tuff cone strata is being altered to soils and is overlain by fall deposits of trachytic pumice.

Table 3
Dominant particle morphology and structures of Facies C–H

Facies	Particle shape	Particle outline	Glass surface structure	Vesicle abundance and shape	Edge modification
C	(1) blocky and equant or splinter-shaped.	(1) linear to slightly irregular due to chipped edges	(1) grain-penetrating fractures, adhering particles, rare chemical pitting	(1) none to very low-spherical	(1) chipped edges, occasional abrading of corners
	(2) blocky angular to elongated (slightly irregular).	(2) linear to weakly concave–convex	(2) adhering particles	(2) very low to high-spherical to ovoid	(2) conchoidal fractures, chipped edges
D	(1) blocky and equant or splinter-shaped.	(1) linear to slightly irregular due to chipped edges	(1) as Facies C but decrease in fractures and increase in chemical pitting	(1) none to very low-spherical	(1) chipped edges and occasional abrading of corners
	(2) blocky to angular or curve-elongated.	(2) linear to very irregular	(2) as (1) and hydration skin and cracks	(2) low to high-spherical	(2) conchoidal fractures
E	(1) blocky, angular or splinter-shaped.	(1) linear to slightly irregular	(1) proximal — few adhering particles. Medial/distal — adhering particles and chemical pitting.	(1) proximal: low to high-spherical. medial/distal: none to very low-spherical to ovoid.	(1) only minor modification (chipped edges)
	(2) blocky, angular or irregular shaped.	(2) linear to weakly concave–convex (Fig. 9C)	(2) as (1) and linear and hydratrion cracks	(2) very low to high-spherical to ovoid	(2) few chipped edges and conchoidal fractures in medial and distal flank
F	(1) blocky and equant; occasional spherical bodies (Fig. 9D).	(1) linear	(1) chemical pitting, adhering particles	(1) none to very low-spherical	(1) only minor modification (chipped edges)
	(2) blocky to angular.	(2) slightly irregular	(2) as (1) and linear cracks, en-echelon fractures	(2) low-spherical to avoid	(2) few conchoidal fractures
G	(1) blocky and equant to angular and splinter shaped.	(1) linear to slightly irregular	(1) few adhering particles and minor chemical pitting	(1) none to very low-spherical	(1) conchoidal fractures
	(2) angular to elongated in proximal deposits and subangular blocky and equant in distal deposits	(2) linear to very irregular	(2) as (1)	(2) none to high-spherical to ovoid	(2) abraded corners and conchoidal fractures
H	(1) blocky and plate-like	(1) linear to slightly irregular	(1) adhering particles and chemical pitting	(1) none to very low-spherical	(1) chipped edges
	(2) blocky and equant to angular	(2) linear to very irregular	(2) as (1)	(2) as (1)	(2) distinct abraded corners, chipped edges and abundant conchoidal fractures

(1) refers to particles ≤ 64 μm and (2) ≥ 64 μm. See Dellino et al. (2001) for description of morphological parameters.

5.4. Section IV — inside the crater

This section represents steeply (~ 38°) dipping deposits inside the crater rim (Figs. 2 and 7F). This section is dominated by crudely stratified deposits (Facies E; Fig. 8 and Table 2) with several beds consisting of embedded clusters of lapilli lenses (Facies B; Fig. 8 and Table 2). Syn- and post-volcanic ring-faulting (displaying several sets of normal faults with a down-throw on the ventward side) and slumping at the crater rim create unconformities between early and late deposits. A small scoria cone and associated lava pond is present inside the crater. The lava pond rests conformably on top of the sedimentary strata (Fig. 7F). Sedimentary deposits are interpreted to be the result of continuous uprush and tephra jets where the lapilli lenses evolved from relatively dry falling tephra.

6. SEM

Fragmentation of magma may occur due to exsolution of gas phases as a result of decompression or by an interaction between external water and the magma (Cashman et al., 2000). These two fragmentation processes produce ash particle with end-members displaying characteristic morphology and surface features (Wohletz, 1983; Heiken and Wohletz, 1985; Büttner et al., 1999; Dellino et al., 2001; Büttner et al., 2002). Dellino et al. (2001) constructed a classification scheme based on features in the literature that are suggested to be diagnostic for phreatomagmatic and magmatic fragmentation. We used this scheme to describe ash particles from the Capelas tuff cone and to interpret the dominant fragmentation process responsible for the deposits. Phreatomagmatic end-members are characterized by a blocky and equant particle shape (Fig. 9A), linear particle outline, quenching cracks and an absence of vesicles. Magmatic end-members are recognized by an irregular particle shape (Fig. 9B), concave–convex particle outline, very high vesicularity and an absence of surface structures such as chemical pitting and adhering particles that are common in phreatomagmatic fragmentation. Intermediate morphologies and structures occur and are described in Dellino et al. (2001). We also note grain modification (Sheridan and Marshall, 1983; Wohletz, 1987) to reveal any differences in emplacement and transport modification within the different facies and sections in the cone. EDS analyses were conducted to verify that interpretations and analyses were carried out on juvenile particles. EDS results were given in standardless composition (weight percent summed to 100% for elements present in concentrations exceeding 1%). Samples were analysed from planar-, diffuse- and crudely stratified deposits (Facies C, D and E respectively), massive to stratified ash deposits (Facies F) undulating ash bed deposits (Facies G) and from massive muddy ash and lapilli (Facies H). 50–200 fine ash (≤ 64 μm) particles were analyzed in each facies. Particles less than 10 μm were not investigated due to image resolution. Samples for SEM were collected from sections I, II, and III (Fig. 2). SEM descriptions are presented in Table 3, dominant particle sizes in Table 4 and interpretations under Section 7.1 (fragmentation processes).

Table 4
Dominant particles sizes in samples of described facies, Table 3

Facies	C	D	E	F	G	H
Dominant particle size (μm)	<10 and >150	<40 and >200	<15 and >200	F.a.: <15 and >200 F.b.: <64	<64	<10 and >150

7. Discussion

7.1. Fragmentation processes

Particles with morphology and textures related to phreatomagmatic fragmentation dominate the deposits of the Capelas tuff cone. Magmatic exsolution of gases, i.e. increased vesicularity, are present in all deposits but only in minor occurrences and generally in grains larger than fine ash. Fine ash is the most important grain size for determining the fragmentation mode (Dellino and La Volpe, 1995; Büttner et al., 1999; Zimanowski et al., 2003). The only findings of particles attributed to magmatic fragmentation in the same amount as phreatomagmatic in the tuff cone strata are in crude stratified deposits (Facies E) in early proximal deposits, section I (Fig. 7B). Magmatic and phreatomagmatic fragmentations are believed to have operated simultaneously due to the occurrence of blocky and equant particles alongside elongated to slightly irregular particles with a high vesicularity of spherical to tubular vesicles. Basaltic eruptions commonly have higher discharge at their outset (Wadge, 1981), which could be responsible for an initially low W/M-ratio. Mixed fragmentation occurs in the transition to a higher W/M-ratio as discharge decreases. Mixed fragmentation could also be due to explosive magma/water interaction in a limited portion of the melt triggering magmatic explosion due to decompression (i.e. creating free space; Dellino et al., 2001) or a vesiculating magma in the central part of a continuous up-rush column (Cole et al., 2001). A lower (more explosive) W/M-ratio also occurred during some periods in the emergent phase of eruption indicated by undulating ash bed deposits (Facies G) emplaced by low

concentration pyroclastic surges. Magmatic fragmentation only dominates in the subaerial last phase when it produced a scoria cone inside the tuff cone. Magmatic end-member particles with contorted and stretched vesicles are found as accidental clasts (trachytic pumice, Fig. 9B) in proximal deposits and at the base of the cone emanating from underlying volcanic units. The grain size is overall larger in proximal deposits and the decrease in grain size and domination of blocky particles with no to very low vesicularity in medial and distal flank deposits (located higher in the stratigraphy; Fig. 8) are evidence for decreasing W/M-ratio and domination of phreatomagmatic fragmentation of higher energy. However, only one investigated bed, massive to stratified ash (Facies F) occurring in the medial section, comprises nearly exclusively phreatomagmatic end-member particles.

The amount of grain surface modification, e.g. chipping and abrasion textures, and mechanical fracturing by grain collision and impact during transport and deposition is not exclusively a factor for interpreting differences between facies (Sheridan and Marshall, 1983) Recycling of particles in the vent area can be very extensive (Kokelaar, 1983; Houghton and Smith, 1993) and thus responsible for parts of the edge modification of grains. However, transport processes within a collisional regime, such as the upper region of a traction carpet in a turbulent pyroclastic surge (Sohn, 1997), are expected to have an increased amount of edge modification (Wohletz, 1983). Facies C, D, G and distal parts of Facies E are by sedimentary structures interpreted in parts to be deposited by pyroclastic surges. Particles from those facies commonly consist of blocky (equant to angular) or splinter-shaped particles exhibiting chipped edges and abraded corners. Conchoidal and grain-penetrating fractures interpreted as mechanical fractures by Wohletz (1987) are also present (generally on larger grains). Larger grains commonly display more abrasion features than do finer particles, which is consistent with the findings of Wohletz (1987). Wohletz (1987) suggested that planar deposits from surges would show an increased amount of edge modification compared to massive and sand-wave surge beds. Planar stratified deposits (Facies C) at the distal flank of the Capelas tuff cone, interpreted as surge deposits, show an almost equal distribution of modification features as found on particles from undulating ash bed deposits (Facies G). Massive to stratified ash (Facies F) shows little edge modification and only rare conchoidal and grain-penetrating fractures, probably related to lateral movement in a waning surge and fallout impact. Some samples of Facies F show similar shape as fallout particles from Surtsey and Capelinhos (Heiken and Wohletz, 1985). Samples from massive muddy ash and lapilli (Facies H), interpreted as reworked deposits, commonly display distinct abraded corners and generally conchoidal fractures. The increased amount of abraded features in Facies H compared to primary deposits is suggested to be the result of secondary transport (i.e. reworking).

7.2. Depositional processes and growth model for the Capelas tuff cone

The growth of the Capelas tuff cone can roughly be divided into three stages based on changes in fragmentation mode and the dominating depositional processes. One stage may include different eruptive episodes and comprise both wet and dry phases.

The first stage consists of the emergence of the tuff cone through seawater and represents a wet Surtseyan–type eruption. The eruption breached the sea surface about 400 m off the pre-existing coastline. Proximal deposits exposed at present sea-level consist dominantly of deposits emplaced by fallout (crudely stratified deposits, Facies E) alternating with minor amounts of undulating base-surge deposits (Facies G), and diffuse stratified deposits (Facies D). These deposits are similar to the fallout deposits described from Surtsey (Kokelaar, 1986), the Ilchulbong tuff cone and the lower part of Udo tuff cone (Sohn and Chough, 1992, 1993; Sohn, 1996). The depositional processes at Capelas likely emanated from dense wet tephra jets (high W/M-ratio) and continuous uprush activity (lower W/M-ratio). The lower W/M-ratio may have occurred during periods with higher magma eruption rate as external seawater was abundant during the first stage. This interpretation is also supported by the high abundance of particles displaying characteristics of magmatic fragmentation mixed with phreatomagmatic particles. As the cone grew larger, particle-laden pyroclastic density currents were able to reach the shoreline. One of the first deposits on pre-existing coastland is an explosion breccia (Facies A) that was probably emplaced by an erosive pyroclastic flow with a head of an advancing ground surge as seen by the discordant contact and associated underlying ash-rich undulating layer. The heterogeneous composition and relatively large grain size (coarse lapilli and bombs, <7 cm in diameter) of the explosion breccia suggests an excavating explosion making the explosion locus deeper and the vent wider. Deposits from the first stage are mainly found in the proximal section (section I) of the tuff cone (Figs. 7A, B and 8). However, lower stratigraphic levels of sections

II and III probably represent distal deposits generated in the first stage of the eruption.

The second stage consists of medial deposits and distal flank deposits, sections II and III respectively (Figs. 7C, D, E and 8). As the eruption progressed, deposits become increasingly finer grained and show distinctly plane-parallel bedding resulting predominantly from emplacement of multiple pyroclastic surges. These surge deposits display strongly grain-segregated layers (planar stratified deposits, Facies C) and undulating deposits (Facies G) (Fig. 7D). The second stage is interpreted as being a less wet system than during the first stage and includes a generally lower W/M-ratio resulting in drier Surtseyan activity. A lower W/M-ratio is supported by an increase in the abundance of pyroclastic surge deposits. These pyroclastic surges are probably associated with an increase of explosion energy during formation of large-scale jets. Large-scale jets produced base surges during the Surtsey and Capelinhos eruptions (Waters and Fisher, 1971; Kokelaar, 1983, 1986). Second-stage deposits located higher up in the strata consist of surge deposits (planar stratified and undulating ash bed deposits, Facies C and G) that alternate with more or less surge-modified fallout deposits (diffuse stratified deposits, Facies D) similar to those of Capelinhos (Cole et al., 2001). Diffuse stratified deposits become increasingly abundant in the higher part of section II (Figs. 7C and 8). Undulating surge beds present in both medial and distal flank deposits display wet features (e.g. plastic deformation) as well as dry features (e.g. strongly grain-segregated layers and brittle behavior when impacted by ballistic ejecta). There is, however, a domination of wet surges. Surge deposits as described in tuff rings, e.g. the Taal, Songaksan and Suwolbong tuff rings (Moore et al., 1966; Waters and Fisher, 1971; Kokelaar, 1986; Sohn and Chough, 1989; Chough and Sohn, 1990; Sohn, 1996), commonly display climbing ripples, megaripples and long wavelengths in sand-wave structures that do not occur at the Capelas tuff cone. The absence of such structures at Capelas suggests that the surges were of lower energy than their tuff ring equivalents. SEM analyses of the fine-ash fraction (<64 μm) show a domination of blocky and equant (to angular) particles produced by phreatomagmatic fragmentation. Similarly shaped particles also dominate the deposits of Surtsey and Capelinhos (Kokelaar, 1986). Large lenses of reworked deposits interbedded with surge and fallout deposits occur at slope breaks in the Capelas tuff cone. These lenses are probably formed during periods of wet eruptions or intense rainfall resulting in remobilization of material by excess water. Reworked deposits are common in many wet tuff cone deposits (Lorenz, 1974a,b; Kokelaar, 1983, 1986; Verwoerd and Chevallier, 1987; Leat and Thompson, 1988; Sohn and Chough, 1992). Steep outward-dipping upper strata (up to 31°), indicating domination of fallout deposits (Sohn, 1996), also display some wet cohesive features with soft-sediment deformation structures and mudflow channels. A horizon with abundant U-channels occurs ~ 3 m above the tuff cone base and can be traced from medial to distal flank deposits (Fig. 6). The horizon was initially carved out by surface runoff eroding the unconsolidated tephra and is interpreted to reflect a period of quiescence in the Capelas eruption. The runoff channels were later modified by base surges (to U-shape rather than V-shape) and infilled with reworked, fallout and base-surge deposits. Deposits and structures present in sections II and III suggest that the first stage of volcanism at Capelas gradually evolved into stage two with an overall lower W/M-ratio (compared to the first stage deposits). We infer this to be the result of repeated partial collapse of cone strata and subsequent build-up of the tephra pile as commonly observed during similar eruptions (Cole et al., 2001).

During the third stage, the tephra pile effectively prevented external water from gaining access to the rising magma in large enough quantities to generate phreatomagmatic explosions. The eruption of the Capelas tuff cone ended during this last stage and these deposits are of magmatic origin, including the build-up of a small scoria cone and emplacement of an associated lava pond inside the tuff cone crater. Syn- and post-eruptive marine erosion has since eroded about 50% of the original tuff cone deposit.

8. Conclusions

The Capelas tuff cone is an emergent Surtseyan-type tuff cone that evolved from wet to drier phreatomagmatic activity during the growth of the cone and ended with a final phase of purely dry magmatic activity (e.g. effusive). This interpretation is based on cone morphology, depositional processes and dominant fragmentation mode recorded in the tuff cone strata. The cone displays steep-sided rim beds (<38° dip inward and <31° dip outward), a crater floor situated 55 m above present sea-level and a relatively high rim height/width ratio (0.15) that is similar to other described tuff cones worldwide. Fallout is the dominant depositional process during the growth of the tuff cone, which is also widely used as one of the characteristics of tuff cones compared to tuff rings (i.e. tuff rings are dominated by surge deposits). As deduced from the stratigraphy, the growth of the Capelas tuff cone can be divided into three main stages. The initial stage at Capelas corresponds well to wet

Surtseyan activity, with a domination of wet fallout and only minor surge deposits. As the cone grew larger, the amount of seawater entering the vent area is suggested to gradually decrease and result in a lower W/M-ratio. The second stage includes a transition from wet deposits to a non-rhythmic oscillation between relatively dry and relatively wet Surtseyan-type activity as seen by the presence of wet fallout deposits, remobilization processes, wet and drier surge deposits and relatively dry fallout deposits (late deposits inside the rim). This is probably due to repeated collapse of the tephra pile material and subsequent build-up of the cone. The third and last stage includes dry magmatic activity that built up a scoria cone and emplaced a lava pond inside the tuff cone crater and finally ending the eruption at Capelas. This stage occurred when the vent area became completely isolated from external water resulting in a final effusive stage.

These results suggest an evolution with time from initial wet Surtseyan activity toward drier Surtseyan activity in the second stage (i.e. lower W/M-ratio) as indicated by the presence of drier surge deposits and later of grain-flow deposits inside the crater rim. However, surge deposits present in the Capelas tuff cone do not correspond to dry surge deposits commonly found in tuff rings (such as the Taal, Suwolbong and Songaksan tuff rings) as they lack features such as climbing ripples, large-scale dune-structures and megaripples. This study is consistent with the conclusions of Sohn (1996) that tuff cones may consist of both wet and dry Surtseyan deposits, but at Capelas with a complement of embedded thin surge deposits rarely displaying dry features. These deposits are probably influenced by variable W/M mass and mixing ratios. The fine ash fraction (<64 μm) of the investigated samples from the Capelas tuff cone deposits is dominated by phreatomagmatic particles. However, particles with magmatic features do occur in all samples and in a large abundance in proximal deposits, suggesting that magmatic and phreatomagmatic fragmentation operated simultaneously.

Acknowledgements

We are grateful for the financial funding from the Department of Geology and Geochemistry at Stockholm University. The study was also supported by grants from the Gavelin fund (to H. Solgevik) and the Lars Hierta Memorial Fund (to H. B. Mattsson). Eve Arnold, Stockholm University, is gratefully acknowledged for comments and discussions on early versions of the manuscript. We would also like to thank Marianne Ahlbom, Stockholm University, for assisting us during SEM imaging and EDS analyses of the Capelas samples. Constructive reviews by Michael Ort and an anonymous reviewer are gratefully appreciated.

References

Aranda-Gómez, J.J., Luhr, J.F., 1996. Origin of the Joya Honda maar, San Luis Potosí, México. J. Volcanol. Geotherm. Res. 74, 1–18.

Büttner, R., Dellino, P., Zimanowski, B., 1999. Identifying magma–water interaction from the surface features of ash particles. Nature 104, 688–690.

Büttner, R., Dellino, P., La Volpe, L., Lorenz, V., Zimanowski, B., 2002. Thermohydraulic explosions in phreatomagmatic eruptions as evidenced by the comparison between pyroclasts and products from Molten Fuel Coolant Interaction experiments. J. Geophys. Res. 107 (B11), 2277, doi:10.1029/2001JB000511.

Cashman, K.V., Sturtevant, B., Papale, P., Navon, O., 2000. Magmatic fragmentation. In: Sigurdsson, H., Houghton, B.F., McNutt, S.R., Rymer, H., Stix, J. (Eds.), Encyclopedia of Volcanoes. Academic Press, pp. 412–430.

Chough, S.K., Sohn, Y.K., 1990. Depositional mechanics and sequences of base surges, Songaksan tuff ring, Cheju Island, Korea. Sedimentology 37, 1115–1135.

Carey, S.T., 1991. Transport and deposition of tephra by pyroclastic flows and surges. In: Fisher, R.V., Smith, G.A. (Eds.), Sedimentation in Volcanic Settings. SEPM. Spec. Publ., vol. 45, pp. 39–57.

Cole, P.D., 1991. Migration direction of sand-wave structures in pyroclastic-surge deposits: implications for depositional processes. Geology 19, 1108–1111.

Cole, P.D., Guest, J.E., Duncan, A.M., Pacheco, J.-M., 1995. An historic subplinian/phreatomagmatic eruption: the 1630 A.D. eruption of Furnas volcano, São Miguel, Azores. J. Volcanol. Geotherm. Res. 69, 117–135.

Cole, P.D., Guest, J.E., Duncan, A.M., Pacheco, J.-M., 2001. Capelinhos 1957–1958, Faial, Azores: deposits formed by an emergent surtseyan eruption. Bull. Volcanol. 63, 204–220.

Connor, C.B., Conway, F.M., 2000. Basaltic volcanic fields. In: Sigurdsson, H., Houghton, B.F., McNutt, S.R., Rymer, H., Stix, J. (Eds.), Encyclopedia of Volcanoes. Academic Press, pp. 331–343.

Crowe, B.M., Fisher, R.V., 1973. Sedimentary structures in base-surge deposits with special reference to cross-bedding, Ubehebe craters, Death Valley, California. Geol. Soc. Amer. Bull. 84, 663–682.

Dellino, P., La Volpe, L., 1995. Fragmentation versus transportation mechanisms in the pyroclastic sequence of Monte Pilato–Rocche Rosse (Lipari, Italy). J. Volcanol. Geotherm. Res. 64, 211–231.

Dellino, P., Isaia, R., La Volpe, L., Orsi, G., 2001. Statistical analysis of textural data from complex pyroclastic sequences: implications for fragmentation processes of the Agnano–Monte Spina Tephra (4.1 ka), Phlegraean Fields, southern Italy. Bull. Volcanol. 63, 443–461.

Dellino, P., Isaia, R., Veneruso, M., 2004a. Turbulent boundary layer shear flows as an approximation of base surges at Campi Flegrei (Southern Italy). J. Volcanol. Geotherm. Res. 133, 211–228.

Dellino, P., Isaia, R., La Volpe, L., Orsi, G., 2004b. Interaction between particles transported by fall-out and surge in deposits of the Agnano Monte Spina eruption (Campi Flegrei, Southern Italy). J. Volcanol. Geotherm. Res. 133, 193–210.

De Rosa, R., Frazzetta, G., La Volpe, L., 1992. An approach for investigating the depositional mechanism of fine-grained surge deposits. The example of the dry surge deposits at "La Fossa di Volcano". J. Volcanol. Geotherm. Res. 51, 305–321.

Druitt, T.H., 1998. Pyroclastic density currents. In: Gilbert, J.S., Sparks, R.S.J. (Eds.), The physics of explosive volcanic eruptions. Geol. Soc. Lond. Spec. Publ., vol. 145, pp. 145–182.

Fisher, R.V., 1977. Erosion by volcanic base-surge density currents: U-shaped channels. Geol. Soc. Amer. Bull. 88, 1287–1297.

Fisher, R.V., Schmincke, H.-U., 1984. Pyroclastic Rocks. Springer–Verlag, Berlin. 474 pp.

Guest, J.E., Gaspar, J.L., Cole, P.D., Queiroz, G., Duncan, A.M., Wallenstein, N., Ferreira, T., Pacheco, J.-M., 1999. Volcanic geology of Furnas Volcano, São Miguel, Azores. J. Volcanol. Geotherm. Res. 92, 1–29.

Heiken, G., Wohletz, K.H., 1985. Volcanic Ash. University of California Press, Berkley. 246 pp.

Houghton, B.F., Smith, R.T., 1993. Recycling of magmatic clasts during explosive eruptions: estimating the true juvenile content of phreatomagmatic volcanic deposits. Bull. Volcanol. 55, 414–420.

Houghton, B.F., Wilson, C.J.N., Pyle, D.M., 2000. Pyroclastic fall deposits. In: Sigurdsson, H., Houghton, B.F., McNutt, S.R., Rymer, H., Stix, J. (Eds.), Encyclopedia of Volcanoes. Academic Press, pp. 555–570.

Jónsson, S., Alves, M.M., Sigmundsson, F., 1999. Low rates of deformation of the Furnas and Fogo volcanoes, São Miguel, Azores, observed with the Global Positioning System, 1993–1997. J. Volcanol. Geotherm. Res. 92, 83–94.

Kokelaar, B.P., 1983. The mechanism of Surtseyan volcanism. J. Geol. Soc. (Lond.) 140, 939–944.

Kokelaar, B.P., 1986. Magma–water interactions in subaqueous and emergent basaltic volcanism. Bull. Volcanol. 48, 275–289.

Leat, P.T., Thompson, R.N., 1988. Miocene hydrovolcanism in NW Colorado, U.S.A., fuelled by explosive mixing of basic magma and wet unconsolidated sediment. Bull. Volcanol. 50, 229–243.

Lorenz, V., 1974a. Studies of the Surtsey tephra deposits. Surtsey Res. Prog. Rep. 7, 72–79.

Lorenz, V., 1974b. Vesiculated tuffs and associated features. Sedimentology 21, 273–291.

Lorenz, V., 1986. On the growth of maars and diatremes and its relevance to the formation of Tuff rings. Bull. Volcanol. 48, 265–274.

Madeira, J., Ribeiro, A., 1990. Geodynamic models for the Azores triple junction. A contribution from tectonics. Tectonophysics 184, 405–415.

Moore, J.G., 1985. Structure and eruptive mechanism at Surtsey Volcano, Iceland. Geol. Mag. 122, 649–661.

Moore, R.B., 1990. Volcanic geology and eruption frequency, São Miguel, Azores. Bull. Volcanol. 52, 602–614.

Moore, G.M., Nakamura, K., Alcaraz, A., 1966. The 1965 eruption of Taal volcano. Science 151, 955–960.

Németh, K., Martin, U., Harangi, Sz., 2001. Miocene phreatomagmatic volcanism at Tihany (Pannonian Basin, Hungary). J. Volcanol. Geotherm. Res. 111, 111–135.

Németh, K., White, J.D.L., Reay, A., Martin, U., 2003. Compositional variation during monogenetic volcano growth and its implications for magma supply to continental volcanic fields. J. Geol. Soc. (Lond.) 160, 523–530.

Ross, G.M., 1986. Eruptive style and construction of shallow marine mafic tuff cones in the Narakay volcanic complex (proterozoic, Hornby bay group, Northwest territories, Canada). J. Volcanol. Geotherm. Res. 27, 265–297.

Scarth, A., Tanguy, J.-C., 2001. Volcanoes of Europe. Terra Publishing, England. 243 pp.

Schmincke, H.-U., 2004. Volcanism. Springer–Verlag, Berlin, Heidelberg. 324 pp.

Searle, R., 1980. Tectonic pattern of the Azores spreading centre and triple junction. Earth Planet. Sci. Lett. 51, 415–434.

Sheridan, M.F., Marshall, J.R., 1983. Scanning electron microscopic examination of pyroclastic materials: basic considerations. Scanning Electron Microscopy. SEM Inc, Chicago, pp. 113–118.

Sheridan, M.F., Wohletz, K.H., 1983. Hydrovolcanism: basic considerations and review. J. Volcanol. Geotherm. Res. 17, 1–29.

Shultz, A.W., 1984. Subaerial debris-flow deposition in the upper Paleozoic Cutler formation, Western Colorado. J. Sediment. Petrol. 54, 759–772.

Sohn, Y.K., 1996. Hydrovolcanic processes forming basaltic Tuff rings and cones on Cheju Island, Korea. Geol. Soc. Amer. Bull. 108, 1199–1211.

Sohn, Y.K., 1997. On traction-carpet sedimentation. J. Sediment. Res. 67, 502–509.

Sohn, Y.K., Chough, S.K., 1989. Depositional processes of the Suwolbong tuff ring, Cheju Island (Korea). Sedimentology 36, 837–855.

Sohn, Y.K., Chough, S.K., 1992. The Ilchulbong tuff cone, Cheju Island, South Korea: depositional processes and evolution of an emergent, Surtseyan-type tuff cone. Sedimentology 39, 523–544.

Sohn, Y.K., Chough, S.K., 1993. The Udo tuff cone, Cheju Island, South Korea: transformation of pyroclastic fall into debris fall and grain flow on a steep volcanic cone slope. Sedimentology 40, 769–786.

Sohn, Y.K., Park, K.H., 2005. Composite Tuff ring/cone complexes in Jeju Island, Korea: possible consequences of substrate collapse and vent migration. J. Volcanol. Geotherm. Res. 141, 157–175.

Storey, M., Wolff, J.A., Norry, M.J., Marriner, G.F., 1989. Origin of hybrid lavas from Agua de Pau volcano, São Miguel, Azores. In: Saunders, A.D., Norry, M.J. (Eds.), Magmatism in the Ocean Basins. Geol. Soc. Spec. Publ., vol. 42, pp. 161–180.

Sumita, M., Schmincke, H.-U., Miyaji, N., Endo, K., 2004. Cock's tail jets and their deposits. In: Németh, K., Martin, U., Goth, K., Lexa, J. (Eds.), Abstract Volume of the Second International Maar Conference. Occ. Pap. Geol. Inst. Hung., p. 94.

Thorarinsson, S., 1967. Surtsey, the New Island in the North Atlantic. The Viking Press, New York. 47 pp.

Thorarinsson, S., Einarsson, Th., Sigvaldason, G., Elisson, G., 1964. The submarine eruption off the Vestmann Islands 1963–64, a preliminary report. Bull. Volcanol. 27, 435–445.

Valentine, G.A., Fisher, R.V., 2000. Pyroclastic surges and blasts. In: Sigurdsson, H., Houghton, B.F., McNutt, S.R., Rymer, H., Stix, J. (Eds.), Encyclopedia of Volcanoes. Academic Press, pp. 571–580.

Verwoerd, W.J., Chevallier, L., 1987. Contrasting types of surtseyan tuff cones on Marion and Prince Edwards islands, southwest Indian Ocean. Bull. Volcanol. 49, 399–417.

Vespermann, D., Schmincke, H.-U., 2000. Scoria cones and tuff rings. In: Sigurdsson, H., Houghton, B.F., McNutt, S.R., Rymer, H., Stix, J. (Eds.), Encyclopedia of Volcanoes. Academic Press, pp. 683–694.

Vogt, P.R., Jung, W.Y., 2004. The Terceira rift as hyper-slow, hotspot-dominated oblique spreading axis: a comparison with other slow-spreading plate boundaries. Earth Planet. Sci. Lett. 218, 77–99.

Wadge, G., 1981. The variation of magma discharge during basaltic eruptions. J. Volcanol. Geotherm. Res. 11, 139–168.

Walker, G.P.L., 1984. Characteristics of dune-bedded pyroclastic surge bedsets. J. Volcanol. Geotherm. Res. 20, 281–296.

Walker, G.P.L., 2000. Basaltic volcanoes and volcanic systems. In: Sigurdsson, H., Houghton, B.F., McNutt, S.R., Rymer, H., Stix, J. (Eds.), Encyclopedia of Volcanoes. Academic Press, pp. 283–289.

Waters, A.C., Fisher, R.V., 1971. Base surges and their deposits: Capelinhos and Taal Volcanoes. J. Geophys. Res. 76, 5596–5614.

White, J.D.L., 1991. The depositional record of small, monogenetic volcanoes within terrestrial basins. In: Fisher, R.V., Smith, G.A. (Eds.), Sedimentation in Volcanic Settings. SEPM. Spec. Publ., vol. 45, pp. 155–171.

White, J.D.L., Houghton, B., 2000. Surtseyan and related phreatomagmatic eruptions. In: Sigurdsson, H., Houghton, B.F., McNutt, S.R., Rymer, H., Stix, J. (Eds.), Encyclopedia of Volcanoes. Academic Press, pp. 495–511.

Wilson, C.J.N., Hildreth, W., 1998. Hybrid fall deposits in the Bishop Tuff, California: a novel pyroclastic depositional mechanism. Geology 26, 7–10.

Wohletz, K.H., 1983. Mechanisms of hydrovolcanic pyroclast formation: grain-size, scanning electron microscopy and experimental studies. J. Volcanol. Geotherm. Res. 17, 31–63.

Wohletz, K.H., 1987. Chemical and textural surface features of pyroclasts from hydrovolcanic eruption sequences. In: Marshall, J.R. (Ed.), Clastic Particles. Van Nostrand Reinhold Company Inc., New York, pp. 79–97.

Wohletz, K.H., Sheridan, M.F., 1979. A model of pyroclastic surge. In: Chapin, C.E., Elston, W.E. (Eds.), Geol. Soc. Am. Spec. Pap., vol. 180, pp. 177–194.

Wohletz, K.H., Sheridan, M.F., 1983. Hydrovolcanic explosions II. Evolution of basaltic Tuff rings and tuff cones. Am. J. Sci. 283, 385–413.

Wohletz, K.H., McQueen, R.G., 1984. Experimental studies of hydromagmatic volcanism. Explosive Volcanism: Inception, Evolution and Hazards. Studies in Geophysics. National Academy Press, Washington, pp. 158–169.

Wood, C.A., 1980. Morphometric evolution of cinder cones. J. Volcanol. Geotherm. Res. 7, 387–413.

Zimanowski, B., Wohletz, K.H., Dellino, P., Büttner, R., 2003. The volcanic ash problem. J. Volcanol. Geotherm. Res. 122, 1–5.